DOI: 10.13009/EUCASS2019-581

Extension of a Non-Adiabatic Flamelet Combustion Model for Composition Predictions in Thermal Boundary Layers

Daniel Rahn[⋆†]*, Hendrik Riedmann*[‡] *and Oskar Haidn*[⋆]

[⋆]*Technische Universität München (TUM), Institute of Turbomachinery and Flight Propulsion (LTF), Boltzmannstr. 15, 85748 Garching, Germany*
[‡]*ArianeGroup GmbH, Robert-Koch-Str. 1, 82024 Taufkirchen, Germany*

daniel.rahn@ltf.mw.tum.de
[†]Corresponding author

Abstract

The fluid species composition plays a vital role in the wall heat transfer prediction and can be significantly impacted by non-adiabatic effects in the vicinity of cooled wall structures. This research work presents an approach to incorporate the underlying physical impact of a temperature dependency in the chemical reaction rates into the flamelet combustion modeling concept. By evaluating the local Damkoehler number, the newly developed methodology dynamically switches between reactive and frozen chemistry to model the regime of slow kinetic processes. It is validated against finite rate simulations for three 2D test cases subjected to a thermal wall boundary condition.

1. Introduction

The incorporation of numerical design and simulation tools is a vital part of the cost reduction efforts in the European space launch industry. By offering insight into specific phenomena not accessible to measurement techniques combined with great flexibility and fast turnaround times, the design and development of rocket propulsion systems can be streamlined. In order to achieve these goals, modeling approaches are used to describe the underlying physical and chemical processes. Before being applied in the industrial development process, these modeling strategies must have been validated for a wide range of typical operating conditions to ensure a high trustworthiness in the prediction of critical parameters. For the design of rocket thrust chambers, such parameters can be given by the heat transfer rate to the combustion chamber wall, the combustion chamber pressure, the combustion efficiency and performance parameters like the specific impulse. The corresponding strategy from sub-scale test data validation to full-scale applications followed by the European space launch provider ArianeGroup has been discussed by *Knab et al.* [6].

The present research work focuses on the wall heat transfer rate as critical design parameter. Its accurate prediction is especially important for the definition of the coolant system which serves to ensure the structural integrity of the rocket thrust chamber. An important requirement is hereby the high fidelity prediction of the local fluid composition together with the thermodynamic and transport data in the respective near wall region as a basis for the heat flux evaluation. While this is consistently achieved for the propellant combination hydrogen - oxygen with the established numerical modeling strategies at ArianeGroup [5, 15], past research works have shown that the same predictive fidelity level for the wall heat flux coupled with other engine characteristics is not reached for the increasingly investigated propellant combination methane - oxygen [2, 16]. Therefore, research efforts within a collaboration between the Technical University of Munich and ArianeGroup funded by the Bavarian Research Foundation are underway to develop and validate new modeling strategies.

Within this project, a non-adiabatic flamelet combustion model has been developed to account for the characteristic large temperature gradients forming a thermal boundary layer near the cooled combustion chamber walls in rocket thrust chambers [14]. This enables the pre-tabulation of the species composition together with thermodynamic and transport data as a function of the local fluid enthalpy. Employing this modeling approach within the ArianeGroup in-house Reynolds-averaged Navier Stokes simulation code *Rocflam3* has however revealed an overprediction of chemical recombination processes in the vicinity of cooled walls leading to a higher wall heat flux estimation. This is due to the intrinsic definition of the flamelet combustion model: It automatically reduces to an equilibrium combustion model

DOI: 10.13009/EUCASS2019-581

in the near wall region as the scalar dissipation rate as non-equilibrium parameter converges towards zero at the wall. This gives the underlying chemical reactions infinite time to reach their equilibrium state, which ultimately leads to an overestimation of recombination processes despite the slow reaction rates in time space. These results are consistent with the observations made by *Perakis et al.* [8, 9] employing a similar non-adiabatic flamelet modeling strategy using a commercial simulation tool.

Based on these results, the existing non-adiabatic flamelet combustion model has been extended to increase the fidelity in the numerical wall heat transfer computation. This extension aims primarily at describing the underlying physical and chemical processes in thermal boundary layers to predict the local fluid composition. Using the resulting physically representative fluid composition together with the derived thermodynamic and transport quantities of the fluid is the foundation for a more accurate wall heat flux prediction.

The newly developed modeling methodology based on computing a local Damkoehler number in the solution field of the *Rocflam3* solver is first introduced in this research work in section 2. For its validation, three representative 2D test cases are defined in section 3 covering the formation, reheating and recirculation patterns in thermal boundary layers. For each case, different operating points in regard to pressure, flow velocity and propellant mixture ratio are investigated to cover the application range of typical sub-scale rocket thrust chamber test cases. The simulations are performed using the classic adiabatic [13], the previously developed non-adiabatic [14] and the newly developed chemical timescale based frozen non-adiabatic flamelet combustion model. The validation is performed against higher fidelity laminar finite rate simulations using the full chemical mechanism during the CFD computation in the commercial solver *Ansys Fluent*. The respective results are given and discussed in section 4 of this paper.

2. Modeling Approach

The new combustion modeling strategy is building up on the fundamental developments presented by *Rahn et al.* [14]. In this previous work, the classic adiabatic flamelet modeling approach based on the concept of *Peters* [10] has been adapted to account for an enthalpy variation as present near cooled rocket thrust chamber walls. This is done by introducing an additional source term $\dot{S}$ into the energy transport equation when solving the counterflow diffusion flame configuration as representation of a locally laminar diffusion flame structure within the flamelet concept. The resulting equation expressed along the physical coordinate x connecting the opposing fuel and oxidizer inlets

$$\rho c_p u \frac{\partial T}{\partial x} = \frac{\partial}{\partial x}\left(\lambda \frac{\partial T}{\partial x}\right) - \sum_i j_i c_{p,i} \frac{\partial T}{\partial x} - \sum_i M_i h_i \dot{\omega}_i + \dot{S} \tag{1}$$

is solved using the chemistry software package *Cantera* [3]. Hereby, ρ, c_p, λ, u and T are the density, heat capacity, heat conductivity, axial velocity and temperature of the fluid mixture respectively. For each species i, j_i represents the diffusive mass flux, M_i the molecular weight and $\dot{\omega}_i$ the production rate from the underlying chemical mechanism [14]. The source term $\dot{S}$ is iteratively adapted using an external numerical empirical algorithm until the enthalpy distribution of the counterflow diffusion flame solution matches an a-priori defined target enthalpy profile $h_{target} = f(x)$. In addition to different target enthalpy profiles, a solution for the counterflow diffusion flame configuration is obtained at different pressure (p) levels and different levels of the scalar dissipation rate (χ) as a non-equilibrium parameter representing the induced strain on the flame structure. The respective solutions are transferred from the physical solution space into the mixture fraction space describing the fluid composition between the two bounds of $Z = 0$ for pure oxidizer and $Z = 1$ for pure fuel. In order to model the turbulence chemistry interaction the 4D laminar flamelet solutions are then integrated using a β-PDF for the mixture fraction, which further introduces a dependency on the mixture fraction variance Z''^2. Ultimately, the counterflow diffusion flame solutions comprising the temperature T, the mixture quantities molar mass M, density ρ, heat capacity c_p, thermal conductivity λ and viscosity μ together with the species composition Y_i are stored in the 5D non-adiabatic flamelet library, which can be expressed mathematically as

$$T, M, \rho, c_p, \lambda, \mu, Y_i = f(Z, Z''^2, \chi, p, h) \ . \tag{2}$$

The newly developed combustion model extends the existing concept in two distinctive ways, which are discussed in the following sections 2.1 and 2.2 before the incorporation into the *Rocflam3* solver is detailed in section 2.3.

2.1 Tabulation of the Chemical Timescale

Within the first extension of the existing non-adiabatic flamelet combustion model, the tabulated dataset as specified in Eq. 2 is extended to include a chemical reaction timescale $\tau_c = f(Z, \chi, p, h)$ as an estimation of how fast the kinetic processes are advancing. The determination of a representative chemical timescale describing the complex combustion

DOI: 10.13009/EUCASS2019-581

physics is still a matter of ongoing research projects. In this context, a common and well-established method for analyzing the chemical timescales of large reaction mechanism is based on an evaluation of the Jacobian Matrix $J_{\dot{\omega}}$ of the chemical species source terms $\dot{\omega}$ [12]. Following an eigenvector decomposition, multiple chemical timescales can be computed based on the relation

$$\tau_i = \frac{1}{|\lambda_i|} \tag{3}$$

using the eigenvalues λ_i for $i = 1, \ldots, N$, where N is the number of species in the reaction mechanism. The difficulty is now to reduce the set of chemical timescales, which can range over several orders of magnitude, into a single characteristic time scale representing the combustion dynamics. Two such approaches have been compared to two new methods being computationally less expensive in the work of *Pruefert et al.* [12]. A novel approach for the chemical timescale computation has been suggested by *Isaac et al.* [4] in order to compute a Damkoehler number distribution. Hereby, a Principal Component Analysis is performed on the solution data of a previous numerical simulation. A backward elimination is then used to discard the species that are highly correlated with the eigenvectors having the smallest eigenvalues. This procedure is continued until the remaining species retain at least 99% of the original data variance in the system forming a new reduced species subset, which is used to define the Jacobian Matrix $J_{\dot{\omega}}$ only including the partial derivatives with respect to the new subset. The latter modeling approach is being adapted and followed for the implementations within this research work. Therefore, the chemical timescales must first be computed based on the computed counterflow diffusion flame solution before a Principal Component Analysis is performed to obtain a single characteristic reaction time scale τ_c.

From the system of differential equations used in the *Cantera* [3] software package, the Jacobian Matrix

$$J_{\dot{Y}} = \begin{bmatrix} \frac{\partial \dot{Y}_1}{\partial Y_1} & \cdots & \frac{\partial \dot{Y}_1}{\partial Y_N} \\ \vdots & \ddots & \vdots \\ \frac{\partial \dot{Y}_N}{\partial Y_1} & \cdots & \frac{\partial \dot{Y}_N}{\partial Y_N} \end{bmatrix} \tag{4}$$

containing the partial derivatives of the rate changing species composition vector $\dot{Y}_i$ with N species can be constructed in a postprocessing step. For each grid point in the 1D solution space, this construction is done by evaluating the perturbed residual within a finite differencing scheme. The obtained derivatives can be correlated to the actual source term $\dot{\omega}_i$ representing the production rate for each species i due to the chemical reactions using the relation

$$\frac{\partial \dot{Y}_i}{\partial Y_j} = \frac{\partial\left(\frac{M_i}{\rho}\dot{\omega}_i\right)}{\partial Y_j} \ . \tag{5}$$

This additionally introduces the mixture density ρ and the molecular weight M_i of the chemical species i. By evaluating the remaining partial derivative and subsequent reordering of the equation, one obtains the general relation

$$\frac{\partial \dot{\omega}_i}{\partial Y_j} = \frac{\rho}{M_i}\frac{\partial \dot{Y}_i}{\partial Y_j} + \frac{\dot{\omega}_i}{\rho}\frac{\partial \rho}{\partial Y_j} \tag{6}$$

for a single matrix element (i, j) of the Jacobian Matrix $J_{\dot{\omega}}$ for the species production rate $\dot{\omega}$. The value of $\dot{\omega}_i$ appearing on the right hand side of the equation is available in the counterflow diffusion flame solution field and a result of the underlying chemical reaction mechanism. The first partial derivative in the previous equation represents the (i, j) element of the Jacobian Matrix $J_{\dot{Y}}$ while the second derivative is the last remaining unknown quantity at this point. It can be computed by assuming the presence of an ideal gas with locally constant pressure p and temperature T for the current analysis point in the 1D solution space giving

$$\frac{\partial \rho}{\partial Y_j} = \frac{p}{RT}\frac{\partial M}{\partial Y_j} \ . \tag{7}$$

Hereby, the universal gas constant R and the molecular weight M of the mixture are introduced. The derivative of the latter can be evaluated using the definition of the mixture molecular weight and applying the quotient rule to obtain

$$\frac{M}{\partial Y_j} = \frac{\partial}{\partial Y_j}\left(\frac{1}{\sum\limits_j \frac{Y_j}{M_j}}\right) = -M^2\frac{1}{M_j} \ . \tag{8}$$

DOI: 10.13009/EUCASS2019-581

Using this result, the Jacobian Matrix of the species production rates can be assembled to

$$J_{\dot{\omega}} = \begin{bmatrix} \frac{\partial \dot{\omega}_1}{\partial Y_1} & \cdots & \frac{\partial \dot{\omega}_1}{\partial Y_N} \\ \vdots & \ddots & \vdots \\ \frac{\partial \dot{\omega}_N}{\partial Y_1} & \cdots & \frac{\partial \dot{\omega}_N}{\partial Y_N} \end{bmatrix} \quad with \quad \frac{\partial \dot{\omega}_i}{\partial Y_j} = \frac{\rho}{M_i} J_{\dot{Y}(i,j)} - \frac{M}{M_j} \dot{\omega}_i \tag{9}$$

and evaluated for each point in the solution domain. Before further processing the data, multiple filtering steps are applied in mixture fraction, enthalpy and scalar dissipation rate space using a Savitzky-Golay Smoothing Filter [17]. This filters high frequency numerical noise resulting from the finite difference computation of the Jacobian Matrix $J_{\dot{Y}}$.

An additional preprocessing step consists of conducting an iterative Principal Component Analysis (PCA) on the counterflow diffusion flame solution vector Y_i of the species composition. The input data is first normalized using the mean value assigning dominant species a higher level of importance. Within the current research, it has been concluded that this provides more reliable results compared to an additional normalization by the standard deviation. In a second step, the eigenvectors and eigenvalues of the Covariance Matrix representing the joint variability between two chemical species for the 1D solution space is computed. A forward selection procedure is then used by picking the original species i with the highest correlation to the first eigenvector (having the highest eigenvalue) into the new subset Y_{PCA} while the respective species is removed from the original solution vector Y_i. The iterative character of the implemented algorithm is then given by computing another PCA on the reduced solution data $Y_i - Y_{PCA}$. This is repeated until the subset Y_{PCA} containing N_{PCA} species retains 99.9% of the original data variance.

Following the determination of the Jacobian Matrix $J_{\dot{\omega}}$ and the completion of the Principal Component Analysis, the chemical timescale to be used in the flamelet manifold can be evaluated according to

$$\tau_c = \left[\frac{M}{\rho} \left(\sum_{i}^{N} \left[\sum_{i_{PCA}}^{N_{PCA}} \dot{\omega}_{i_{PCA},norm} \, J_{\dot{\omega},(i,i_{PCA})} \right]^2 \right)^{0.5} \right]^{-1} \tag{10}$$

with an additional importance weighting by the normalized magnitude of the reactive species source term.

The results of this computational process are visualized for an exemplary dataset in Fig. 1. The graphic shows the dependency of τ_c on the temperature T, the pressure p and the oxidizer fuel ratio O/F as a different expression for the mixture fraction $Z = 1/(1 + O/F)$. One can see that the chemical timescale increases exponentially with decreasing temperature indicating a slowdown of the reactive processes. Furthermore, the chemical reactions proceed slower at lower pressure values. Regarding the oxidizer fuel ratio, the chemical timescale at the same pressure and temperature becomes larger towards stoichiometry at $O/F = 4$ except for lower temperatures. However, the maximum temperature in the flame increases in this direction which is generally coupled with smaller minimum values of τ_c.

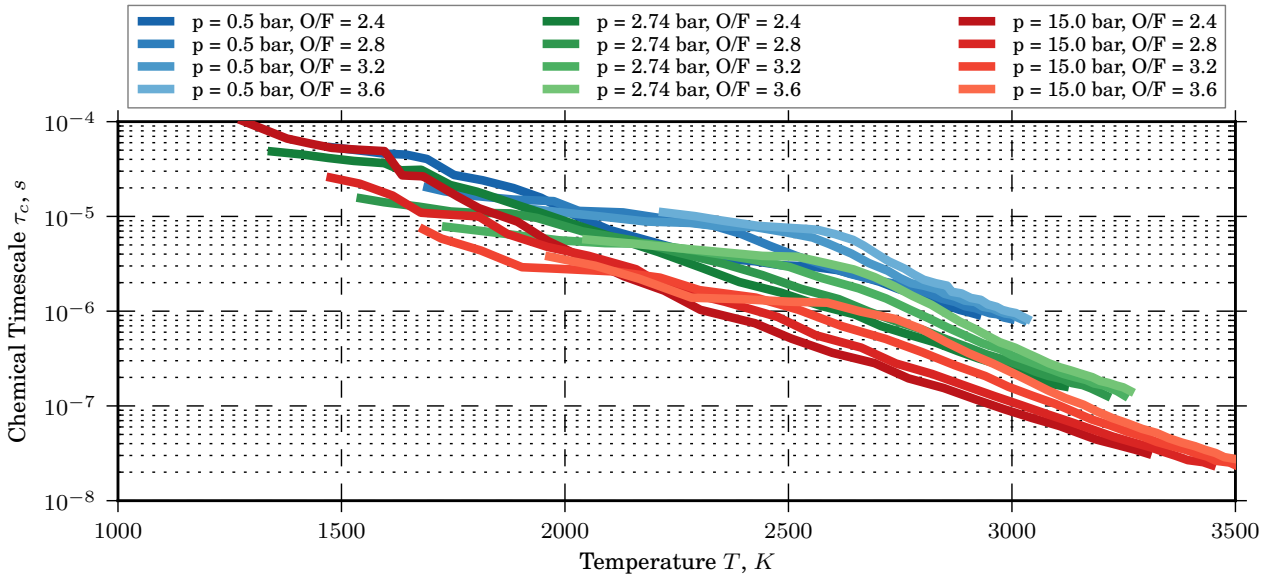

Figure 1: Chemical timescale as a function of the temperature for different combinations of constant pressure and oxidizer fuel ratio as stored in the non-adiabatic flamelet library.

DOI: 10.13009/EUCASS2019-581

2.2 Frozen Extension of the Tabulated Flamelet Data

The second step in order to define the new combustion model is the extension of the tabulated dataset as specified in Eq. 2 by a 6th dimension on which the tabulated thermodynamic and transport data depends: the frozen enthalpy h_f. This variable definition is required as the chemistry library is expanded to include a "frozen" flamelet data branch for which the respective species composition remains constant. In order to uniquely identify the species composition from which the chemical freezing occurs, the frozen enthalpy is introduced referring to the respective original enthalpy level. The regular enthalpy h is then varied towards lower values for each frozen enthalpy level. The corresponding data structure for the enthalpy flamelet manifold is sketched in Fig. 2 where the enthalpy values decrease along positive axis directions. Along the line marked by the red dots, the flamelet solution from the counterflow diffusion flame configuration is stored. For these points, the condition $h = h_f$ is satisfied. The blue dots indicate the data of the frozen model extension for which the species composition remains constant along lines of $h_f = const.$ for decreasing enthalpy.

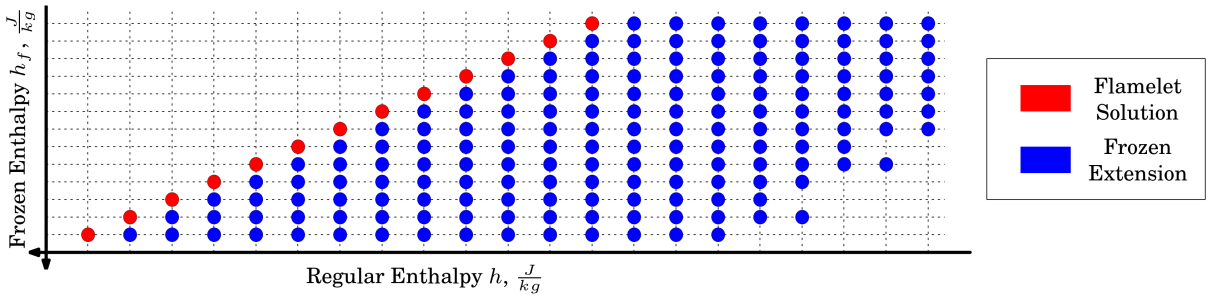

Figure 2: Schematic visualization of the enthalpy data structure for the extended 6D flamelet chemistry library for a combination of constant Z, Z''^2, χ and p.

As the species composition Y_i and as a consequence the molar mass M of the mixture remain constant, it is only necessary to compute a new temperature distribution to fully describe the frozen extension of the 6D flamelet manifold. This is due to the fact that the remaining variables given by the density ρ, heat capacity c_p, thermal conductivity λ and viscosity μ can be fully reevaluated in this case. The new temperature solution profiles are computed using a Newton algorithm. By searching the root of the enthalpy error function including an analytical expression for the derivative based on the NASA polynomial expressions, the procedure

$$T_{i+1} = T_i - \frac{f(T_i)}{\frac{\partial f(T_i)}{\partial T}} \quad with \quad f(T) = h(T) - h_{target} = 0 \tag{11}$$

is executed until convergence is achieved. The procedure is applied to all flamelet enthalpy levels for all combinations of the defining variables Z, Z''^2, χ and p to fully span the 6D frozen flamelet manifold.

2.3 Model Implementation in the CFD Solver

The modeling extensions introduced in sections 2.1 and 2.2 take effect during the preprocessing step of the chemical reaction mechanism using the counterflow diffusion flame configuration. The resulting 6D chemical timescale based frozen non-adiabatic flamelet manifold is then provided as a tabulated input to the *Rocflam3* CFD solver enabling an efficient solution due to the decoupling of the combustion and flow computations. By using the extended input, the impact of chemical kinetic rate effects can be incorporated into the numerical simulation. The governing dimensionless number to assess the impact of the reaction rates is given by the Damkoehler number

$$Da = \frac{\tau_f}{\tau_c} \tag{12}$$

as ratio of the fluid timescale τ_f and the chemical reaction timescale τ_c. In regions of large Damkoehler numbers, the chemical reactions proceed fast compared to the fluid or mixing times. Therefore, the reactive flow is governed by flow or mixing effects and a locally laminar flame structure is present within the smallest turbulent structures. The respective region of $Da > 1$ is therefore also the validity region of the classic flamelet modeling approach. However, an application in thermal boundary layers as present in rocket thrust chambers can violate this limit as the reaction timescale τ_c becomes larger with decreasing temperature as the data in Fig. 1 shows. When approaching the region of

DOI: 10.13009/EUCASS2019-581

$Da \approx 1$, chemical kinetic rate effects become dominant in describing the combustion process in a turbulent flow. Due to the slower reaction rates, the rate change in the species composition vector $\dot{Y}_i$ is not able to follow the fluid flow anymore. On a global perspective, the fluid composition "freezes" for $Da < 1$ and remains approximately constant along the streamlines of the fluid velocity vector field.

The newly developed combustion modeling approach implemented in the ArianeGroup in-house CFD solver *Rocflam3* intends to model this physical phenomenon. Therefore, the Damkoehler number must be evaluated for all finite volumes of the numerical solution domain. The chemical timescale τ_c is obtained by linear interpolation from the previously discussed flamelet manifold. The local fluid time scale is computed as the minimum of the integral turbulent timescale $\tau_{f,int}$, the Kolmogorov timescale $\tau_{f,\eta}$ and a diffusion timescale $\tau_{f,diff}$ defined by the equations

$$\tau_{f,int} = \frac{k}{\epsilon} \quad , \quad \tau_{f,\eta} = \sqrt{\frac{\mu}{\rho\epsilon}} \quad and \quad \tau_{f,diff} = \frac{\rho c_p}{\lambda}\sqrt{\frac{\mu^3}{\epsilon\rho^3}} \tag{13}$$

with k as the turbulent kinetic energy and ϵ as the dissipation rate of turbulent energy. Using these definitions, both convective and diffusion processes can be considered for the Damkoehler number evaluation. While the first two equations represent the time to dissipate energy in the large and small scale eddies respectively, the chosen definition of $\tau_{f,diff}$ represents the time thermal and mixing diffusion processes require based on the Kolmogorov length scale and is related to the Batchelor scale [1].

With the computed Damkoehler number, the transition from the fluid flow dominated combustion regime to the reaction rate dominated regime can be modeled in *Rocflam3*. For this purpose, a blending function Da_{blend} is introduced to ensure a smooth transition from the reacting counterflow diffusion flame data to the frozen chemistry data branch in the 6D precomputed manifold. The large Damkoehler number regime in which the regular flamelet applies is defined by $Da > 10$ and the blending function has a constant value of $Da_{blend} = 1$. On the other side, the small Damkoehler number regime representing the frozen chemistry data branch is defined by $Da < 0.1$ for which $Da_{blend} = 0$ is being set in the solver. In order to ensure a smooth blending in the intermediate region $0.1 \leq Da \leq 10$, the function definition for Da_{blend} is derived from the inverse tangent function $tan^{-1}(Da)$ depending on the local Damkoehler number.

Ultimately, an additional transport equation must be introduced into *Rocflam3* for the previously defined frozen enthalpy h_f. Its local value represents the enthalpy level at which the transition to the low Damkoehler number regime has potentially occurred upstream of the current finite volume. It thereby refers to the respective species composition at which the reaction rates have become too small to induce a significant change. Based on its definition, the frozen enthalpy h_f is equal to the local fluid enthalpy h in regions of large Damkoehler numbers Da. After the transition to frozen chemistry has occurred, the variable h_f is simply transported with the global fluid flow and therefore subjected to convective and diffusive transport processes. These physical considerations regarding the behavior of h_f lead to the definition of the following transport equation

$$\frac{\partial(\rho\, u\, h_f)}{\partial x} = \lambda\frac{\partial^2 T}{\partial x^2} + \dot{Q}_{h_f} \tag{14}$$

derived from the regular enthalpy transport equation being implemented into *Rocflam3*. It includes the definition of a source term

$$\dot{Q}_{h_f} = \dot{m}(h - h_f)Da_{blend} \tag{15}$$

governing the characteristic development of the frozen enthalpy solution field by using the mass flow rate $\dot{m}$. While Da_{blend} is equal to 1 for large Damkoehler numbers, h_f follows the spatial development described by the standard enthalpy transport equation to ensure $h_f = h$. With the transition to $Da_{blend} \rightarrow 0$, the source term $\dot{Q}_{h_f}$ approaches 0 and the pure transport of the frozen enthalpy is modeled by its transport equation.

3. Test Case Definition

For a validation of the previously introduced modeling approach, three simplified 2D test cases based on a flat plate configuration are defined. These target the investigation of thermal boundary layer characteristics under rocket thrust chamber operating conditions by looking closer at different phenomena in each test case. Test case number 1 and 2 share the same geometry definitions while differing only in the temperature wall boundary condition. For case 1, the pure cool down of the hot combustion gases along the flat plate is investigated. A similar cooling along the wall is first enforced in case 2, but is followed by a reheating section to investigate the return from frozen chemistry to active reaction kinetics. Moving away from pure flat plate flow conditions, test case 3 enables the investigation of a developing recirculation zone similar to the injection conditions in rocket thrust chambers. This is enforced by creating a backward facing step for the hot combustion chamber gases at the inlet boundary condition. In the following, the different test cases and operating points together with the computational setup are introduced in greater detail.

DOI: 10.13009/EUCASS2019-581

3.1 Geometry and Boundary Conditions

The main computational plane for each of the three cases is given by the x-y plane in the 3D space with the geometric dimensions as outlined in Fig. 3 (a) and (b). In general, the defined computational domains are characterized by a large length to height ratio as the thermal boundary layer forming along the wall at $y = 0\,\text{m}$ is the primary focus of this research work. For test case 3 depicted in Fig. 3 (b), the domain length is shortened as the recirculation zone is the primary focus of the investigation. To initiate the formation of this recirculation zone, the backward facing step dimension is given by $\Delta y = 0.005\,\text{m}$ or $\frac{1}{6}$th of the full geometric height of $Y_{geom} = 0.03\,\text{m}$.

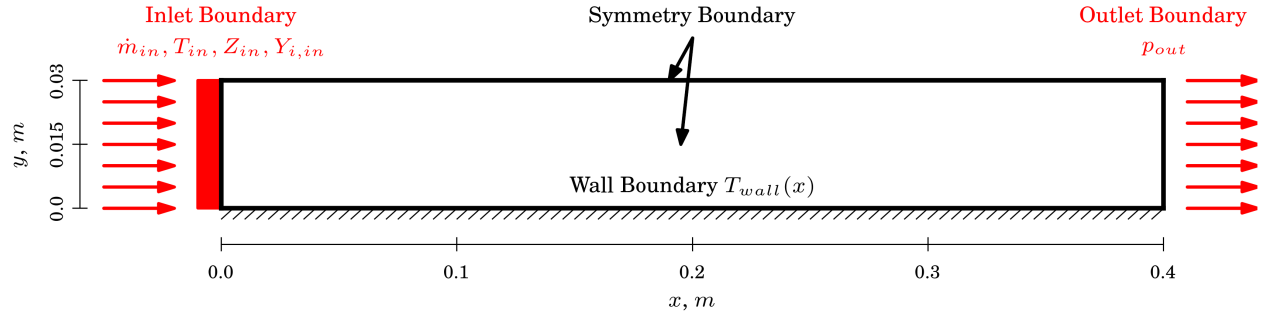

(a) Thermal boundary layer test cases number 1 and 2.

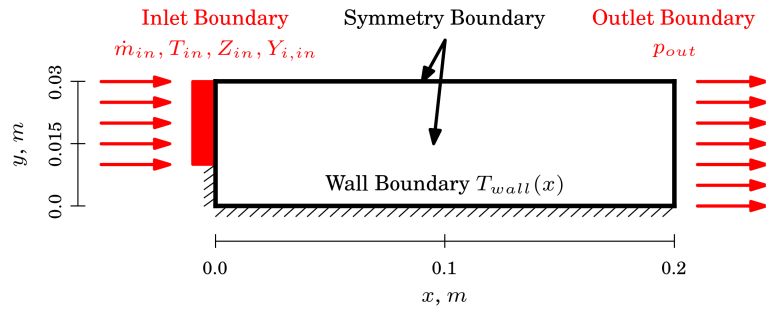

(b) Recirculation zone test case number 3.

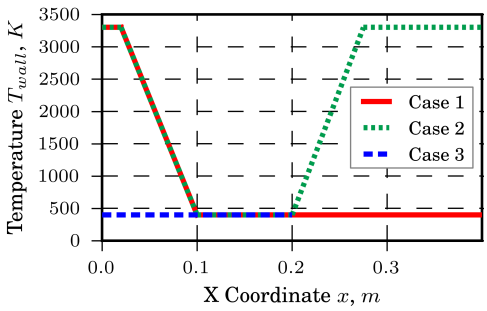

(c) Temperature function at wall boundary.

Figure 3: Geometry and boundary condition definitions.

For the given surface definitions in Fig. 3, the corresponding individual boundary conditions are set identically in the *Rocflam3* and *Ansys Fluent* solver. The side surfaces of the configurations are defined by a symmetry boundary condition. The same boundary condition type is enforced at the top surface of the simulation domains. In combination, the defined flat plate setups therefore represent a channel geometry of infinite width and a height of $2 \times Y_{geom}$. For the inlet boundary condition, a constant mass flow rate $\dot{m}_{in}$ is set for a mixture of hot combustion gases based on the propellant combination methane - oxygen (CH_4-O_2). By choosing a pre-combusted inlet flow, the impact of different predictions for the initial combustion process by the different modeling approaches can be reduced. This enables a focus on the specific phenomena to be investigated. In addition to the mass flow, a constant static temperature T_{in} is enforced at the inlet. While this can be directly done using *Rocflam3*, an external user defined function is used to dynamically define the total inlet temperature in *Ansys Fluent* to ensure a constant value of T_{in}. The respective value is given by the predicted flamelet combustion temperature at adiabatic conditions. Regarding the chemistry modeling approach in each solver, the inflow conditions must be set as well. For the flamelet combustion models used in the *Rocflam3* solver a constant mixture fraction value Z_{in} is provided. After the respective simulations have been conducted, the average fluid composition $Y_{i,in}$ is transferred as inlet boundary condition for the laminar finite rate combustion model in *Ansys Fluent*. This procedure ensures the definition of equal species compositions at the inlet for all simulations. At the outlet plane of the geometry, a constant static pressure p_{out} is defined with a value depending on the targeted operating condition. Ultimately, the wall temperature distribution T_{wall} for each case is plotted in Fig. 3 (c) as a function of the x coordinate of the geometry. The higher temperature value is the adiabatic combustion temperature depending on the operating point while the cooled wall section has a constant temperature of $T_{wall} = 400\,\text{K}$. For the backward facing step wall segment at $x = 0\,\text{m}$ in test case 3 an adiabatic wall boundary condition is defined.

DOI: 10.13009/EUCASS2019-581

3.2 Operating Points

Three characteristic variables are used to uniquely identify 36 operating points for each of the defined numerical test cases with a summary given in Fig. 4. The respective points represent typical data ranges as they can be observed e.g. in the experimental investigations of the single and multi-element sub-scale rocket thrust chambers operated at the Technical University of Munich [18, 19]. This data range association shall facilitate the modeling validation for future numerical simulations of these test cases.

First, the outlet pressure p_{out} is used to establish a general target pressure level at which the chemical kinetic processes are analyzed. The applied data range in this research work tries to cover three distinctive regimes for rocket thrust chamber applications: the combustion chamber at a representative higher pressure of about 15 bar, an intermediate pressure of 2.5 bar as present in the thrust chamber throat region and a lower pressure value of about 0.5 bar to represent the initial expansion process in a diverging sub-scale rocket nozzle. The second variable is given as the oxidizer fuel ratio O/F to investigate the influence of the propellant mixture ratio. For the model validation in this research work, the slightly fuel rich region as typical operating domain of a rocket thrust chamber is covered (CH_4-O_2 stoichiometry at $O/F = 4$). As a third variable to characterize a single operating point, the average inlet velocity over the full geometric height of $Y_{geom} = 0.03$ m is used. Hereby, the data range correlates with the represented thrust chamber regions for the given pressure value p_{out}. While smaller velocities are being investigated for the elevated combustion chamber pressure, the operating points at lower pressures are characterized by higher velocities to resemble the flow conditions through a converging - diverging rocket thrust chamber geometry. By using $U_{in,avg}$ to identify the operating point instead of the enforced constant mass flow rate $\dot{m}_{in}$ applied for an operating point group in the numerical computation, a corresponding variation as a function of the O/F at constant pressure can be seen in Fig. 4. This is due to the underlying change in the fluid density, which is driven primarily by a change in the hot gas species composition.

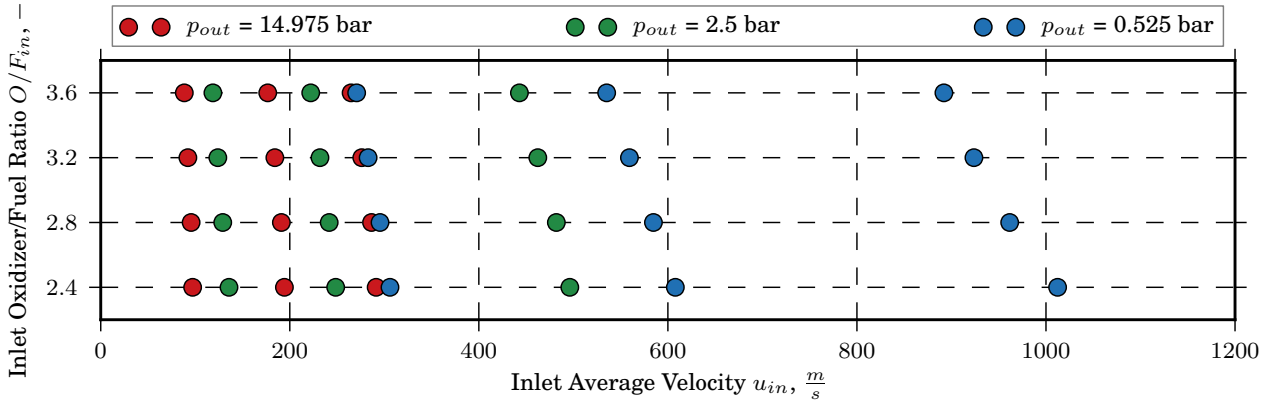

Figure 4: Investigated operating points for the simplified 2D test cases.

In addition to the discussed three variables, it shall be noted that the variation of the pressure level and the oxidizer fuel ratio implies a variation of the adiabatic combustion temperature used to define T_{in} and T_{wall}. This dependent quantity is however not used to characterize the operating points in this research work. Furthermore, the higher velocity operating points at lower pressures are neglected for test case 3 due to a lacking relevance for rocket thrust chamber injection cases. This concerns the combinations $p_{out} = 0.5$ bar with $u_{in} \approx 950\,\mathrm{m\,s^{-1}}$ and $p_{out} = 2.5$ bar with $u_{in} \approx 500\,\mathrm{m\,s^{-1}}$ reducing the respective number of operating points to 28.

3.3 Computational Setup

Both employed solver packages *Rocflam3* and *Ansys Fluent* solve the 3D Favre-averaged Navier-Stokes Equations for mass, momentum and enthalpy by treating the gas phase as a continuous Eulerian phase. This set of differential equations is applied to the previously defined test cases in a quasi 2D approach instead of solving the pure 2D transport equations. Therefore, the computational domain normal to the *x*-*y* plane is resolved by a single finite volume with an enforced symmetry boundary condition on its sides to model the 2D character. In the *x*-*y* plane, the geometry is discretized into finite volumes using a structured grid as shown in Fig. 5. For all test cases, refinement is employed towards the wall boundary condition to ensure the non-dimensional wall distance y^+ satisfies the criteria $y^+ < 1$ to enable a high fidelity gradient evaluation. Additionally, the computational grid for test case 3 is further refined in the recirculation zone region and around the shear layer region following the inlet boundary condition.

DOI: 10.13009/EUCASS2019-581

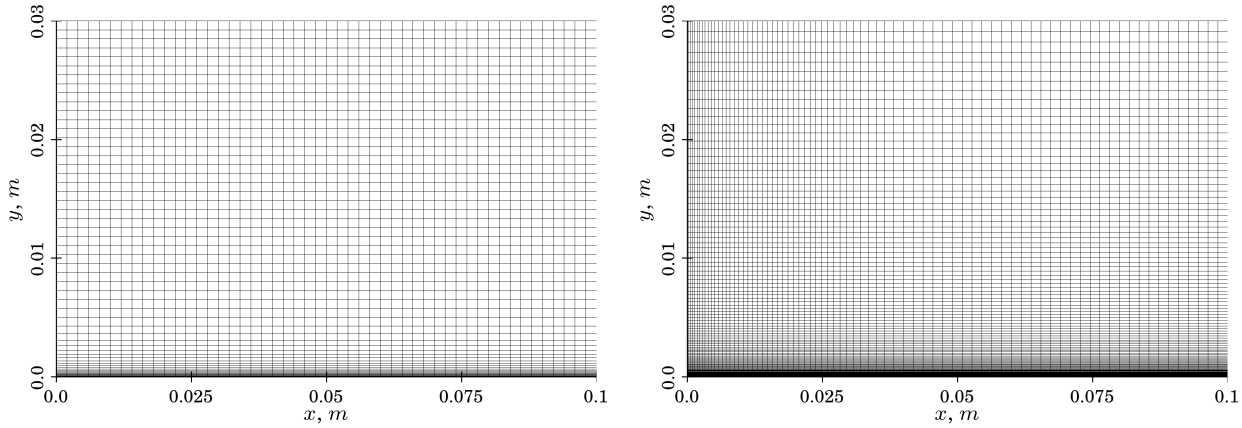

(a) Flat plate geometry for test cases 1 and 2.

(b) Backward facing step geometry for test case 3.

Figure 5: Computational grid for the defined test cases shown in the range 0 m ≤ x ≤ 0.1 m.

A grid convergence study is conducted in order to quantify the numerical error introduced by the chosen finite volume resolution of the geometry. Therefore, the results obtained on different grid resolutions employing the non-adiabatic flamelet combustion model in *Rocflam3* are compared to the solution on the finest resolution. This is done for the quantities temperature T, specific heat capacity c_p, density ρ, thermal conductivity λ, velocity u in x direction and the species composition Y_i taking the major species CO, CO_2, H_2, H_2O and OH into account. For each grid resolution level, this analysis is first done along multiple lines at constant x coordinates. The solution profiles along these lines are projected to a reference grid resolution with logarithmic spacing, therefore placing more analysis points within the boundary layer region. For each of these points, the local relative error ϵ to the finest grid solution is computed before being averaged over all points. At this stage, the five considered chemical species are combined into a single average error value. In a second step, the different relative error values are averaged again over the different analysis positions along the x axis. Further averaging is ultimately applied over the selected operating points investigated at a pressure level of p_{out} = 1 bar. This analysis procedure returns a single relative error value ϵ for each quantity and grid resolution enabling a graphical analysis of the grid convergence as plotted in Fig. 6 for the test cases 1 and 3.

For the geometry used in test cases 1 and 2, the numerical error of the grid resolution is generally at a very low level except for extreme coarsening as the data in Fig. 6 (a) shows. This is due to the fact that the grid resolution normal to the wall is bounded by an upper limit to ensure the criteria $y^+ < 1$ is satisfied for all operating points. In this finite volume size region, additional refinement does not significantly affect the results while only a very coarse resolution in x direction or large computational cells at higher y values lead to an increase in the numerical error. For test case 3 however, the grid resolution in the recirculation and shear layer region additionally impacts the results as indicated in Fig. 6 (b). As soon as the respective phenomena are resolved with sufficient accuracy, the numerical error compared to the finest resolution sharply declines. Based on this analysis, the grid resolution previously shown in Fig. 5 is further used for the simulations using *Rocflam3* and *Ansys Fluent*. It is marked by the red dashed line in Fig. 6. The respective grids contain 11800 finite volumes for the test cases 1 and 2 and 14388 finite volumes for test case 3.

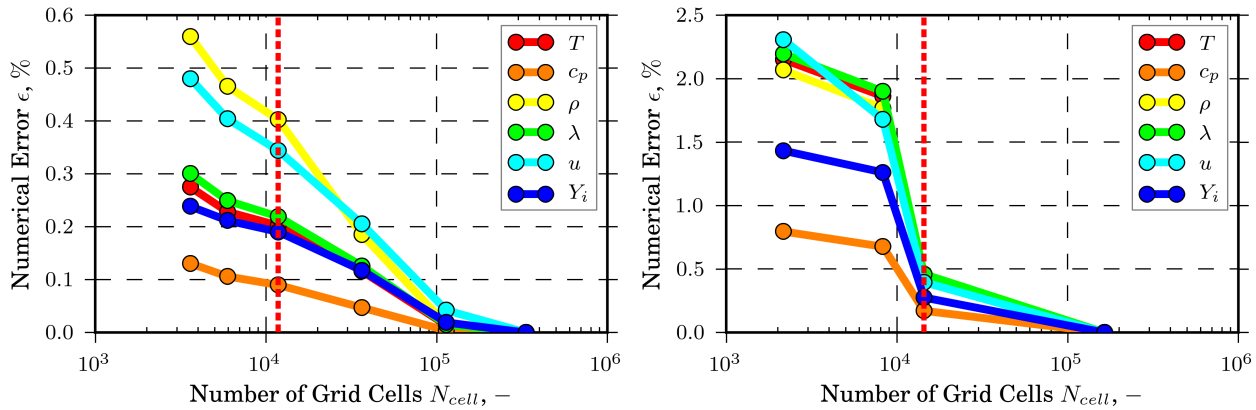

(a) Flat plate geometry for test case 1.

(b) Backward facing step geometry for test case 3.

Figure 6: Numerical error as function of the number of finite volumes for different solution variables.

DOI: 10.13009/EUCASS2019-581

Regarding the general numerical setup in both solvers, the turbulence is modeled using the two equation Shear Stress Transport (SST) model based on the work of Menter [7]. The incorporated model parameters given by the turbulent Schmidt and Prandtl number are set as $Sc_t = 0.7$ and $Pr_t = 0.85$ respectively. The required turbulence intensity as fluctuation from the mean velocity at the inlet boundary condition is defined as 5%. Additionally, second order accuracy in the numerical flux calculation is ensured in *Rocflam3* and *Ansys Fluent*. Regarding the modeling of the chemical kinetic processes, four different approaches are investigated in this research work. Three are based on the flamelet modeling concept of Peters [10] and are implemented into the ArianeGroup in-house solver *Rocflam3* while the laminar finite rate solutions using the commercial *Ansys Fluent* solver serve as the higher fidelity reference data. For all considered combustion modeling approaches, the GRI-3.0 natural gas reaction mechanism with 325 chemical reactions and $N = 53$ species in its original format is used as an input [20]. In order to obtain the laminar finite rate solution, all chemical reactions must be evaluated in every iteration of the CFD solver while $N - 1$ additional transport equations are solved. Hereby, the species Ar, C_3H_7 and C_3H_8 and their reactions are neglected in the standard implementation of *Ansys Fluent*. In order to speed up the laminar finite rate calculation process, the In-Situ Adaptive Tabulation (ISAT) approach is used [11]. For the tabulated flamelet chemistry in *Rocflam3*, previously published methodologies are followed to create an adiabatic [13] and a non-adiabatic [14] chemistry library. Ultimately, the previously introduced modeling approach in section 2 completes the set of four investigated combustion modeling concepts.

The previously introduced definition of the wall temperature $T_{wall} = 400\,\mathrm{K}$ together with the defined operating points can trigger the condensation of certain fluid components, e.g. H_2O. This becomes especially relevant for the low pressure operating points at $p_{out} = 0.5\,\mathrm{bar}$. The transition to the liquid phase is however neglected within the numerical setup in both CFD solvers and the fluid is fully treated as an ideal gas.

4. Results

The numerical simulations of the simplified test cases defined in section 3 are performed using three modeling approaches in the ArianeGroup in-house simulation tool *Rocflam3*: a classic adiabatic flamelet model, a non-adiabatic flamelet model and the newly developed chemical timescale based frozen (T.F.) non-adiabatic flamelet model presented in section 2. For validation purposes, additional simulations are performed with a laminar finite rate combustion model using the commercial *Ansys Fluent* solver together with the full chemical reaction mechanism. For a more detailed analysis of the different predictions in a highly non-adiabatic reactive flow, a single operating point is chosen and the respective results are discussed in section 4.1. This is followed by a global view on the simulation results in section 4.2 comparing the relative error characteristics across all previously defined operating points.

4.1 Single Case Discussion

For the purpose of a more detailed analysis, the operating point given by an outlet pressure of $p_{out} = 14.975\,\mathrm{bar}$, an inlet velocity of $u_{in} = 184.2\,\mathrm{m\,s^{-1}}$ and an oxidizer fuel ratio of $O/F = 3.2$ is chosen. It represents the possible conditions in a sub-scale rocket combustion chamber, for which the prediction of the wall heat transfer characteristics is of high importance. In the following, the Fig. 7 - 9 share a similar structure differing mainly by the different analysis positions of constant x coordinates for the respective test cases. For a comparison of the different combustion modeling approaches, wall normal profiles for the species mass fractions CO and CO_2 are plotted using a solid and dashed line respectively. For an additional visualization of the thermal boundary layer, the temperature profile is plotted using the data from the laminar finite rate simulations.

Within the frame of test case 1, the hot combustion gases are subjected to a low temperature boundary condition representing the cooled wall structure of a rocket thrust chamber leading to the formation of a thermal boundary layer. The resulting wall normal data is plotted in Fig. 7 at two axial positions of the simulation domain. These analysis positions represent the development region of the thermal boundary layer at $x = 0.08\,\mathrm{m}$ and its fully developed state at $x = 0.3\,\mathrm{m}$. For both analysis positions, the core flow composition not affected by the thermal wall boundary condition is practically identical for all numerical simulations and represents the pre-combusted inlet composition. Towards the wall at lower y coordinates, the species composition predictions significantly differ for the different modeling approaches. As one can expect when using the adiabatic flamelet model, the species composition remains constant across the thermal boundary layer as the chemistry library is independent of the fluid enthalpy. For the non-adiabatic flamelet combustion model, the recombination processes between CO and CO_2 are overpredicted as the model converges towards an equilibrium state in the near wall region. This gives the slow recombination reactions infinite time to proceed leading to the results shown in Fig. 7. The species composition only reaches a frozen state after having reached the lowest flamelet enthalpy level for which a valid counterflow diffusion flame solution was obtained before extinction is observed. The given results show that these two modeling approaches are not able to predict a physical species composition as critical input for a wall heat transfer evaluation within a thermal boundary layer region. Based on their

DOI: 10.13009/EUCASS2019-581

definitions, they cannot take into account kinetic rate effects leading to a frozen species composition when the reaction rates become to small as predicted by the higher fidelity laminar finite rate combustion model using the full reaction mechanism. However, the data in Fig. 7 shows that the newly developed T.F. non-adiabatic flamelet model is able to replicate the underlying physical processes within a thermal boundary layer region. For the large Damkoehler number regime at higher temperatures, the predicted species compositions using the two enthalpy dependent flamelet models are practically identical. However, their predictions begin to differ for lower temperatures as the chemical timescale τ_c increases as previously shown in Fig. 1. This leads to a reduction of the local Damkoehler number until approaching the critical value $Da = 1$ around which the reaction rate effects become dominant. By transitioning to the frozen flamelet data branch in this regime, the new combustion model is able to predict the physical freezing process. This significantly reduces the error compared to the higher fidelity model.

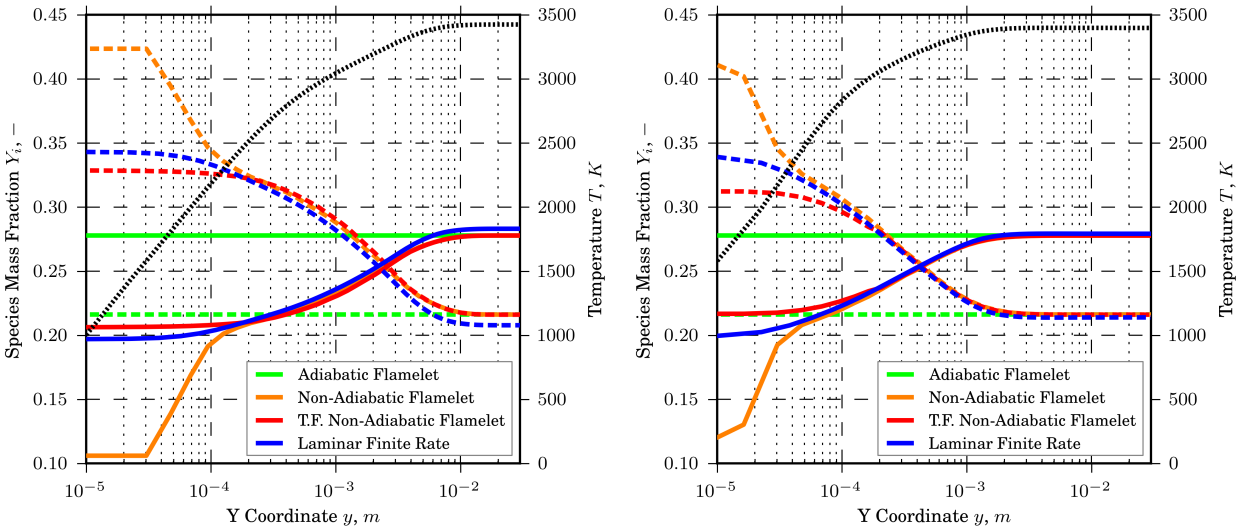

(a) Developing thermal boundary layer at $x = 0.08$ m. (b) Fully developed thermal boundary layer at $x = 0.3$ m.

Figure 7: Test case 1: Wall normal species composition of CO (solid line) and CO_2 (dashed line) and temperature distribution (dotted line).

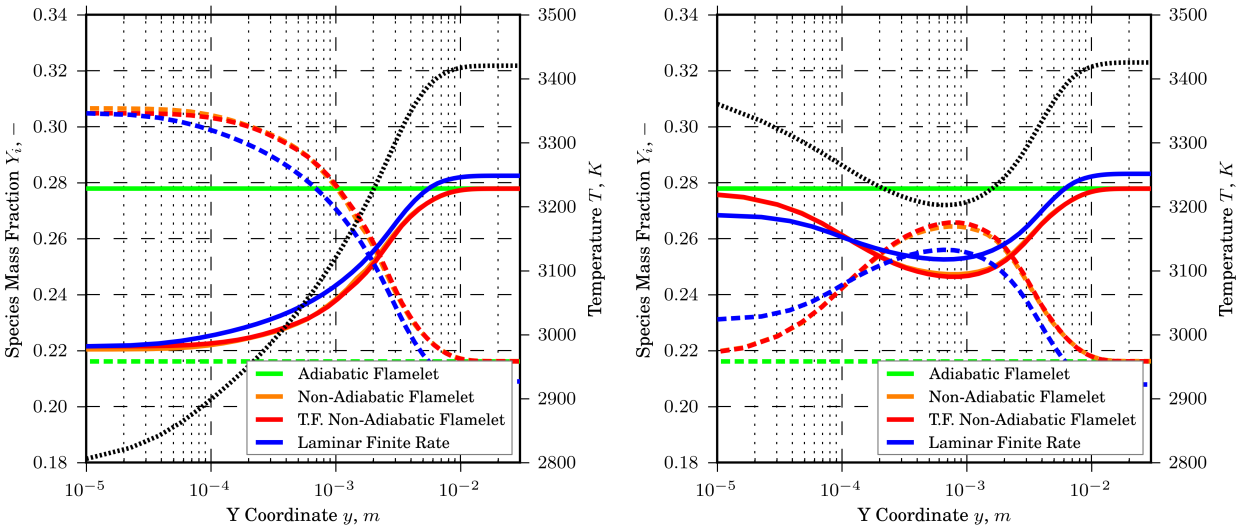

(a) Developing reheating layer at $x = 0.26$ m. (b) Advanced reheating layer at $x = 0.3$ m.

Figure 8: Test case 2: Wall normal species composition of CO (solid line) and CO_2 (dashed line) and temperature distribution (dotted line).

Based on the definition of test case 2, similar characteristics as discussed in regard to Fig. 7 can first be observed for the initial development of a thermal boundary layer. However, for $x > 0.2$ m the wall temperature increases again initiating a transition back to faster chemical reactions with the heat source originating at $y = 0$ m. In order to analyze

DOI: 10.13009/EUCASS2019-581

the different combustion modeling predictions for this flow phenomenon, the analysis positions for the wall normal distributions plotted in Fig. 8 are chosen to show the transition region and an advanced state. Both graphics show characteristic mass fraction profiles that correlate with the respective temperature distributions as a consequence of the wall reheating. While the predictions using the adiabatic flamelet model are still unaffected by these thermal boundary layer effects, both non-adiabatic flamelet approaches give practically equal results as the Damkoehler number increases again due to the faster reaction rates at higher temperatures. Both approaches are able to follow the numerical solution of the higher fidelity combustion model as the data in Fig. 8 shows. This test case confirms the ability of the new modeling approach to correctly return to a reactive state after frozen conditions have occurred upstream.

For the discussion of test case 3 the corresponding x coordinates for the analysis are chosen to show the influence of the combustion model within a fluid flow subjected to a recirculating pattern following a backward facing step. Therefore, the first plot in Fig. 9 (a) shows the wall normal profiles shortly after the inlet plane cutting through the recirculation zone. The dimension of this zone is indicated by the dashed black line marking the y coordinate at which the velocity u in x direction is equal to $0\,\mathrm{m\,s^{-1}}$. Further towards the wall, negative values for the velocity u are observed. The second plot in Fig. 9 (b) shows the data further downstream as the recirculation zone transitions into a regular thermal boundary layer leading to a reversal of the near wall fluid velocity u. Both data sets indicate that the assumption of adiabatic conditions leads to a significant error in the near wall species composition due to the presence of non-adiabatic effects. For the shear layer region between the main hot gas flow and the recirculation zone, the original non-adiabatic model neglecting the impact of the Damkoehler number and the laminar finite rate solution predict an almost equal species composition. The prediction using the new combustion model slightly deviates from the higher fidelity reference solution as the enthalpy drop leading to larger chemical timescales is paired with smaller fluid timescales in the shear layer region, which inflicts the local transition to a partly frozen chemistry. Towards the wall however kinetic rate effects become more important as the fluid temperature drops, an effect that can only be predicted using the new flamelet modeling approach. Further downstream of the recirculation zone, a similar thermal boundary layer pattern as discussed in regard to test case 1 and Fig. 7 develops. This serves as a first confirmation of the applicability of the new combustion model to the typical coaxial injection patterns in rocket thrust chambers.

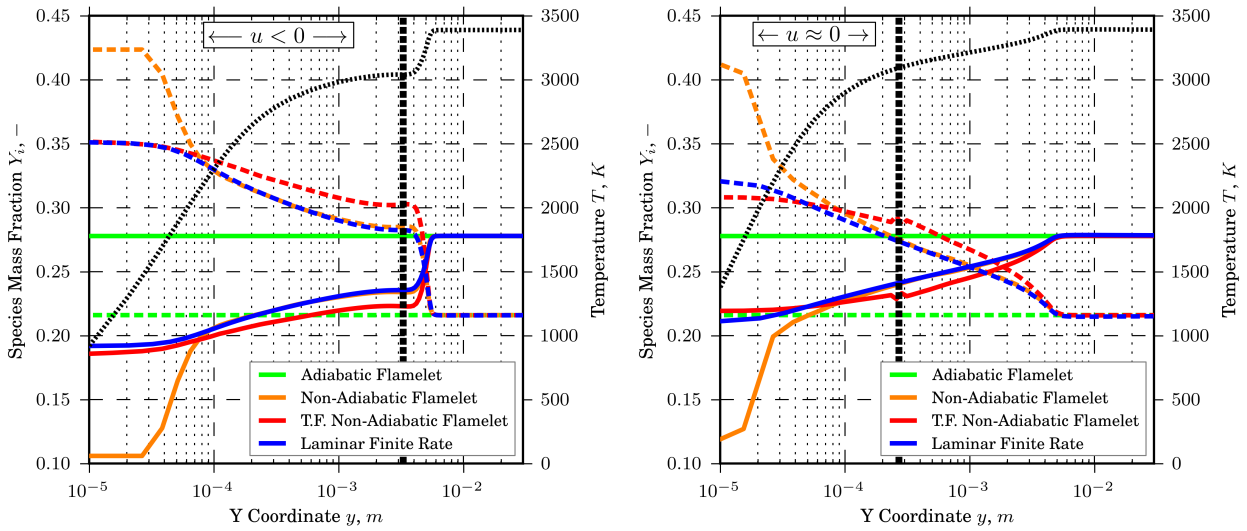

(a) Recirculation zone at $x = 0.005$ m.

(b) Transition region from the recirculation zone to a thermal boundary layer at $x = 0.025$ m.

Figure 9: Test case 3: Wall normal species composition of CO (solid line) and CO_2 (dashed line) and temperature distribution (dotted line).

4.2 Global Analysis

The definition of the three test cases and 36 (test case 1 and 2) or 28 (test case 3) operating points in section 3 creates an analysis domain covering a total of 100 simulations for each of the four considered combustion modeling approaches. As the general trend regarding the prediction of the species composition for the more detailed wall normal distributions discussed in section 4.1 does not significantly change across the defined operating point range, the following analysis reduces the individual differences into global error expressions. The underlying analysis procedure for this global

DOI: 10.13009/EUCASS2019-581

comparison of the different combustion modeling approaches is based on evaluating the species composition of the major species CO, CO_2 and H_2O along the wall boundary condition. It therefore represents the critical composition for a possible subsequent wall heat transfer evaluation. For each test case, the respective values along the wall are extracted within a certain x coordinate range given by

$$0.05\,\mathrm{m} < x < 0.35\,\mathrm{m}\ (1) \quad , \quad 0.2\,\mathrm{m} < x < 0.35\,\mathrm{m}\ (2) \quad \textit{and} \quad 0.0025\,\mathrm{m} < x < 0.1\,\mathrm{m}\ (3) \tag{16}$$

covering the investigated specific flow phenomena. In a first step, the local relative error of each considered species between the three flamelet modeling approaches with respect to the higher fidelity laminar finite rate simulation is computed as a function of x. In the following, the respective data for each test case and operating point is averaged in x space considering the previously defined analysis ranges. Ultimately, this data is averaged across all specified operating points to obtain the global error metrics for each test case as summarized in Tab. 1. The same process is applied to obtain the averaged mass fraction percentage given in the last column representing the contribution of the three considered species CO, CO_2 and H_2O to the overall fluid mass.

Table 1: Species mass fraction error ϵ and the represented mass fraction percentage averaged across all operating points in the specific analysis range for each defined test case.

Test Case	Combustion Model	$\epsilon_{Y_{CO}}$, %	$\epsilon_{Y_{CO_2}}$, %	$\epsilon_{Y_{H_2O}}$, %	$\frac{Y_{CO}+Y_{CO_2}+Y_{H_2O}}{\sum_i^N Y_i}$, %
1	Adiabatic Flamelet	27.2	35.6	11.5	88.5
	Non-Adiabatic Flamelet	32.8	36.9	2.8	95.6
	T.F. Non-Adiabatic Flamelet	6.9	9.4	2.1	96.8
2	Adiabatic Flamelet	14.5	18.4	7.8	88.5
	Non-Adiabatic Flamelet	11.5	12.5	3.5	92.3
	T.F. Non-Adiabatic Flamelet	4.8	6.3	3.2	92.5
3	Adiabatic Flamelet	41.2	32.1	11.6	88.7
	Non-Adiabatic Flamelet	40.5	36.8	2.5	95.5
	T.F. Non-Adiabatic Flamelet	8.4	7.1	1.7	97.1

The additionally computed average mass fraction percentage in the last column of Tab. 1 shows that the consideration of the three species CO, CO_2 and H_2O for the global analysis is a reasonable simplification. Due to their large share of the total fluid mass, these species have a large influence on the heat transfer relevant mixture quantities like the specific heat capacity or thermal conductivity. Therefore, their prediction is a critical input for a reliable wall heat transfer analysis. Furthermore, the laminar finite rate reference computations consistently return averaged values greater than the given flamelet solution results confirming the validity of this selection.

The given data for the considered three species in Tab. 1 clearly indicates an improvement in the species composition prediction when using the newly developed chemical timescale based frozen (T.F.) non-adiabatic flamelet model compared to the other flamelet modeling approaches. As already discussed in section 4.1, the classic adiabatic flamelet model is not suited for an application in highly non-adiabatic flow conditions leading to the given large relative error values. By introducing an enthalpy dependency into the pretabulated flamelet manifold, the average relative error in the H_2O mass fraction distribution can be reduced. However, the respective errors for the CO and CO_2 mass fraction remain at a high level as the slow recombination reactions are allowed to proceed until reaching equilibrium conditions. This leads to an overestimation of Y_{CO_2} in the near wall region while Y_{CO} is underestimated compared to the higher fidelity simulation, which is being reflected by the high average error levels in Tab. 1. Only by taking the underlying kinetic rate effects with the new combustion model into account, the global relative error for the wall species composition can be significantly reduced for all three major combustion products. Nonetheless, using the new combustion model still introduces a small error in the species composition prediction compared to the laminar finite rate simulations. Especially for operating points at lower pressure p_{out}, higher inlet velocity u_{in} and higher mixture ratio O/F, the predictions using the new combustion model start to deviate from the reference solutions. Primarily driven by the very small fluid time scales for these operating points, the transition from flamelet chemistry to frozen composition is predicted too early. Therefore, the non-adiabatic impact on the predicted species mass fraction distributions using the new model is underestimated.

DOI: 10.13009/EUCASS2019-581

5. Summary and Conclusion

A new combustion modeling approach is presented in this research work to extend the flamelet modeling concept to thermal boundary layers in which chemical reaction rate effects dominate the local fluid composition. The new numerical simulation model is based on evaluating the local Damkoehler number as a ratio of the fluid and chemical timescales in the solution field of the CFD solver. For an efficient evaluation, the chemical timescale is being pretabulated during the flamelet chemistry library generation process. Therefore, a new methodology is implemented using the Jacobian Matrix of the chemical species source terms considering only the partial derivatives with respect to a relevant species subset. This subset is determined from a statistical computation using an iterative Principal Component Analysis algorithm. The introduction of the frozen enthalpy to form a 6D flamelet manifold incorporating a data branch of constant species composition completes the preprocessing steps for the decoupled chemistry calculations. Using this as an input for the CFD solver, the dimensionless Damkoehler number serves as a criterion to switch between regions of reaction and fluid flow dominated regimes and therefore allows for the consideration of reaction rate effects within the flamelet modeling concept. This completes the definition of the new chemical timescale based frozen non-adiabatic flamelet combustion model presented in this research work.

The newly developed model is further applied to three simplified 2D test cases covering the following specific phenomena: the formation of a thermal boundary layer through the cool down of hot combustion gases (1), the reheating and return to active chemical reactions of such a thermal boundary layer (2) and the interaction of a recirculation zone and a thermal boundary layer following a backward facing step as present for typical rocket injectors (3). These test cases and their operating points are defined in this research work allowing for a comparison of four different combustion modeling approaches. An adiabatic flamelet model, a non-adiabatic flamelet model and the new chemical timescale based frozen non-adiabatic are compared to higher fidelity laminar finite rate simulations solving the full chemical reaction mechanism. The respective analysis results show that the newly developed combustion model is able to significantly improve the prediction of the fluid composition in the near wall region compared to the existing flamelet modeling concepts, which is a critical enabler for a reliable wall heat transfer analysis in rocket thrust chambers. The physical effect of a slowdown in the reaction rates in thermal boundary layers can be reproduced while significantly lowering the computational effort compared to the higher fidelity simulations. The required CPUh investment is approximately 95% lower when using the new flamelet based combustion modeling approach. It is therefore a promising approach for an industrial scale analysis of rocket thrust chambers which will be further investigated in the near future.

6. Acknowledgment

The authors greatly acknowledge the financial funding for this research work by the Bavarian Research Foundation within a project targeting an increased understanding of the green propellant combination liquid oxygen - methane (“Umweltfreundliche Treibstoffkombination LOX/Methan”). The additional support work on the ArianeGroup side was performed within the national technology program TARES 2020. This program is sponsored by the German Space Agency, DLR Bonn, under contract No. 50RL1710.

References

[1] G.K. Batchelor. Small-scale variation of convected quantities like temperature in turbulent fluid Part 1. General discussion and the case of small conductivity. *Journal of Fluid Mechanics*, 5(1):113–133, 1959.

[2] D. Eiringhaus, D. Rahn, H. Riedmann, O. Knab, and O. Haidn. Numerical Investigation of a 7-Element GOX/GCH4 Subscale Combustion Chamber. In *7th European Conference for Aeronautics and Space Sciences (EUCASS)*, 2017.

[3] D.G. Goodwin, H.K. Moffat, and R.L. Speth. Cantera: An object- oriented software toolkit for chemical kinetics, thermodynamics, and transport processes, version 2.3.0. `www.cantera.org`, Version 2.3.0, 2017.

[4] B. J. Isaac, A. Parente, C. Galletti, J. N. Thornock, P. J. Smith, and L. Tognotti. A Novel Methodology for Chemical Time Scale Evaluation with Detailed Chemical Reaction Kinetics. *Energy & Fuels*, 27:2255–2265, 2013.

[5] B. Ivancic, H. Riedmann, and M. Frey. Validation of Turbulent Combustion Models for the 3D-Simulations of Liquid H2/O2 Rocket Combustors. In *Space Propulsion Conference 2012*, 2012.

DOI: 10.13009/EUCASS2019-581

[6] O. Knab, H. Riedmann, B. Ivancic, C. Hoeglauer, M. Frey, and T. Aichner. Consequences of Modeling Demands on Numerical Rocket Thrust Chamber Flow Simulation Tools. In *6th European Conference for Aeronautics and Space Sciences (EUCASS)*, 2015.

[7] F.R. Menter. Two-Equation Eddy-Viscosity Turbulence Models for Engineering Applications. *AIAA Journal*, 32(8):1598–1605, 1994.

[8] N. Perakis, C. Roth, and O. Haidn. Development of a Non-Adiabatic Flamelet Model for Reacting Flows with Heat Loss. In *Space Propulsion Conference 2018*, 2018.

[9] N. Perakis, C. Roth, and O. Haidn. Simulation of a Single-Element Rocket Combustor using a Non-Adiabatic Flamelet Model. In *Space Propulsion Conference 2018*, 2018.

[10] N. Peters. Laminar diffusion flamelet models in non-premixed turbulent combustion. *Progress in Energy and Combustion Science*, 10(3):319–339, 1984.

[11] S.B. Pope. Computationally efficient implementation of combustion chemistry using in situ adaptive tabulation. *Combustion Theory and Modelling*, 1:41–63, 1997.

[12] U. Pruefert, F. Hunger, and C. Hasse. The analysis of chemical time scales in a partial oxidation flame. *Combustion and Flame*, 161(2):416–426, 2014.

[13] D. Rahn, D. Eiringhaus, H. Riedmann, R. Behr, and O. Haidn. Characterization of an Adiabatic Flamelet Combustion Model for Gaseous CH4/O2 Combustion in Rocket Thrust Chambers. In *Space Propulsion Conference 2018*, 2018.

[14] D. Rahn, O. Haidn, H. Riedmann, and R. Behr. Non-Adiabatic Flamelet Modeling for the Numerical Simulation of Methane Combustion in Rocket Thrust Chambers. In *AIAA Propulsion and Energy Forum, Joint Propulsion Conference*, 2018.

[15] H. Riedmann, B. Kniesner, M. Frey, and C.D. Munz. Modeling of Combustion and Flow in a Single Element GH2/GO2 Combustor. *CEAS Space Journal*, 6:47–59, 2014.

[16] C. Roth, O. Haidn, A. Chemnitz, T. Sattelmayer, Y. Daimon, G. Frank, H. Mueller, J. Zips, M. Pfitzner, R. Keller, P. Gerlinger, D. Maestro, B. Cuenot, H. Riedmann, and L. Selle. Numerical Investigation of Flow and Combustion in a Single-Element GCH4/GOX Rocket Combustor. In *AIAA Propulsion and Energy Forum, Joint Propulsion Conference*, 2016.

[17] A. Savitzky and M.J.E. Golay. Smoothing and Differentiation of Data by Simplified Least Squares Procedures. *Analytical Chemistry*, 36(8):1627–1639, 1964.

[18] S. Silvestri, M.P. Celano, G. Schlieben, and O.J. Haidn. Characterization of a multi-injector gox-gch4 combustion chamber. In *52nd AIAA/SAE/ASEE Joint Propulsion Conference*. AIAA, 2016.

[19] S. Silvestri, M.P. Celano, G. Schlieben, O.J. Haidn, and O. Knab. Comparison of Single Element Rocket Combustion Chambers with Round and Square Cross Section. In *6th European Conference for Aeronautics and Space Sciences (EUCASS)*, 2015.

[20] G.P. Smith, D.M. Golden, M. Frenklach, N.W. Moriarty, B. Eiteneer, M. Goldenberg, T.C. Bowman, R.K. Hanson, S. Song, W.C. Gardiner Jr., V.V. Lissianski, and Z. Qin. GRI-Mech 3.0. `www.me.berkeley.edu/gri_mech`, 2018.